51st IEEE Conference on Decision and Control
December 10-13, 2012. Maui, Hawaii, USA

Rotational and translational bias estimation based on depth and image measurements

Nadège Zarrouati-Vissière, Pierre Rouchon and Karine Beauchard

***Abstract*— Constant biases associated to measured linear and angular velocities of a moving object can be estimated from measurements of a static environment by embedded camera and depth sensor. We propose here a Lyapunov-based observer taking advantage of the $SO(3)$-invariance of the partial differential equations satisfied by the measured brightness and depth fields. The resulting observer is governed by a non-linear integro/partial differential system whose inputs are the linear/angular velocities and the brightness/depth fields. Convergence analysis is investigated under C^3 regularity assumptions on the object motion and its environment. Technically, it relies on Ascoli-Arzela theorem and pre-compacity of the observer trajectories. It ensures asymptotic convergence of the estimated brightness and depth fields. Convergence of the estimated biases is characterized by constraints depending only on the environment. We conjecture that these constraints are automatically satisfied when the environment does not admit any rotational symmetry axis. Such asymptotic observers can be adapted to any realistic camera model. Preliminary simulations with synthetic image and depth data (corrupted by noise around 10%) indicate that such Lyapunov-based observers converge for much weaker regularity assumptions.**

I. Introduction

The problem of estimating the position and the orientation of a moving object such as a ground, an aerial or an underwater vehicle has been extensively studied since World War II. In the 1950's, expensive inertial measurement units (IMUs) were developed, as missile guidance and control required extremely accurate navigation data [1]. Tactical grade IMUs, less expensive, enable dead-reckoning techniques over short time periods, but require position fixes provided by GPS [2], or combination through data fusion of other sensors outputs [3], [4]. As to recent low-cost IMUs using MEMS technologies, the cumulated error due to the bias of gyroscopes integrated over long time periods induces drift in orientation, which can be managed; but from accelerometers, only high frequency output (dynamics) can be relied on. As odometers and velocimeters (e.g. Doppler radar [5], Pitot tube, electromagnetic (EM) log sensor), are commonly available technologies in vehicles, mass market applications can combine their linear velocity outputs with angular velocity from low-quality IMUs. Unfortunately, Pitot probes and EM log sensors are known to only provide air-speed and speed-through-the-water (STW) instead of speed-over-ground (SOG). We intend to study the situation, where linear and angular velocity are provided up to a slowly varying bias (the wind or an ocean current), which can be illustrated by [6].

Our approach leans on vision techniques: the field of dynamic vision mainly focuses on the estimation of motion of a camera and structure of a scene from a sequence of images [7], [8]. It usually tracks feature points between images and simultaneously recovers their three-dimensional (3D) position and the ego-motion of the camera through extended Kalman filtering (simultaneous localization and motion, SLAM) [9] or non-linear observers [10], [11], [12]. Two difficulties systematically arise in those methods: as monocular systems can only estimate translation up to a scale factor, an additional output is required [13]; perspective systems induce nonlinearities to the system dynamics, which forces to study other geometrical formulations (e.g the essential space [14], the Plücker coordinates [15]).

The Kinect device has been a huge outbreak in the robotics and vision communities ([16]) as it provides depth measurements registered at each pixel of a RGB image, at a relatively low cost. To our knowledge, there are few attempts to exploit simultaneously image and dense depth data.

The contributions of this paper can be summarized as follows. We propose an original method to estimate constant biases on angular and translational velocities and, in the same time, to filter the image and depth data. This method relies on an $SO(3)$-invariant partial differential system [17], [18] coupling, for a static environment, the brightness field perceived by a spherical camera, the depth field and the angular/translational velocities. The observer design is based on a Lyapunov functional. It yields an integro/partial differential system for the estimated fields and biases (see (8) for fields on the entire sphere $\mathbb{S}^2$ and see (17) for an adaptation to fields localized on a spherical cap). Asymptotic convergence is investigated under C^3 regularity assumptions on object motions and environment (theorem 2). Simulations (figures 6 and 7) show that such observers could be used with noisy fields and an environment with only a C^0 regularity.

Section II is devoted to the $SO(3)$-invariant model, the partial differential system coupling brightness and depth fields and the C^3 regularity and geometric assumptions used for the observer convergence analysis. In section III, the Lyapunov-based nonlinear observer is introduced and its

Nadège Zarrouati is with DGA, 7-9 rue des Mathurins, 92220 Bagneux, France, PHD candidate at Mines-ParisTech, Centre Automatique et Systèmes, Unité Mathématiques et Systèmes 60, boulevard Saint-Michel 75272 Paris Cedex, France nadege.zarrouati@mines-paristech.fr

Pierre Rouchon is with Mines-ParisTech, Centre Automatique et Systèmes, Unité Mathématiques et Systèmes 60, boulevard Saint-Michel 75272 Paris Cedex, France pierre.rouchon@mines-paristech.fr

Karine Beauchard is with CNRS and CMLS, Ecole Poytechnique, Route de Saclay, 91120 Palaiseau Cedex, France karine.beauchard@math.polytechnique.fr

978-1-4673-2066-5/12/$31.00 ©2012 IEEE

convergence is investigated. In section IV, we explain how to adapt this observer to a realistic pinhole camera model with restricted fields of view, and we present simulations illustrating robustness to noise of 10%.

II. The $SO(3)$-invariant model

A. Modelling and regularity assumptions

The model is based on geometric assumptions introduced in [17], [18]. They are recalled in this sub-section. The camera is spherical. Its motion is given through the linear and angular velocities $v(t)$ and $\omega(t)$ expressed in a reference frame attached to the camera: the camera frame. More precisely, the position of the optical center in the reference frame $\mathcal{R}$ is denoted by $C(t)$. Orientation versus $\mathcal{R}$ is given by the quaternion $q(t)$: any vector ς in the camera frame corresponds to the vector $q\varsigma q^*$ in the reference frame $\mathcal{R}$ using the identification of vectors as imaginary quaternions. We have thus: $\dot{q} = \frac{1}{2}q\omega$ and $\dot{C} = qvq^*$. A pixel is labeled by the unit vector η in the camera frame: η belongs to the sphere $\mathbb{S}^2$ and receives the brightness $y(t,\eta)$. Thus at each time t, the image produced by the camera is described by the scalar field $\mathbb{S}^2 \ni \eta \mapsto y(t,\eta) \in \mathbb{R}$.

The scene is modeled as a closed, C^3 and convex surface Σ of $\mathbb{R}^3$, diffeomorphic to $\mathbb{S}^2$. The camera is inside the domain $\Omega \subset \mathbb{R}^3$ delimited by $\Sigma = \partial\Omega$. To a point $M \in \Sigma$ corresponds one and only one camera pixel. At each time t, there is a bijection between the position of the pixel given by $\eta \in \mathbb{S}^2$ and the point $M \in \Sigma$. Since the point M are labelled by $s \in \mathbb{S}^2$, this means that for each t, exist two mapping $\mathbb{S}^2 \ni s \mapsto \eta = \phi(t,s) \in \mathbb{S}^2$ and $\mathbb{S}^2 \ni \eta \mapsto s = \psi(t,\eta) \in \mathbb{S}^2$ with $\phi(t,\psi(t,\eta)) \equiv \eta$ and $\psi(t,\phi(t,s)) \equiv s$, for all $\eta, s \in \mathbb{S}^2$. To summarize we have:

$$\eta := q(t)^* \frac{\overrightarrow{C(t)M(s)}}{\|\overrightarrow{C(t)M(s)}\|} q(t) \text{ and } s = \psi(t,\eta) \tag{1}$$

where $\psi(t,.)$ and $\phi(t,.)$ are diffeomorphisms of $\mathbb{S}^2$ for every $t > 0$.

The density of light emitted by a point $M(s) \in \Sigma$ does not depend on the direction of emission (Σ is a Lambertian surface) and is independent of t (the scene is static). This means that $y(t,\eta)$ depends only on s: there exists a function $y_\Sigma(s)$ such that

$$y(t,\eta) = y_\Sigma(\psi(t,\eta)). \tag{2}$$

The distance $\|\overrightarrow{C(t)M(s)}\|$ between the optical center and the object seen in the direction $\eta = \phi(t,s)$ is denoted by $D(t,s)$, and its inverse by $\Gamma = 1/D$

$$\Gamma(t,\eta) := \frac{1}{\|\overrightarrow{C(t)M(\psi(t,\eta))}\|}. \tag{3}$$

Fig.1 illustrates the model and the notations.

We assume

1) v and ω are C^2 functions of $t \in [0,+\infty)$ and their derivatives are uniformly bounded up to order 2 with respect to $t \geq 0$,
2) y_Σ is a C^3 function of $s \in \mathbb{S}^2$,

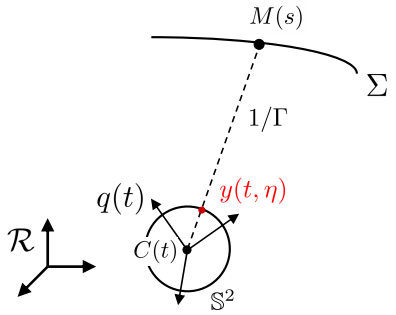

Fig. 1. Model and notations of a spherical camera in a static environment [17], [18].

3) $C(t)$ stays in a fixed compact subset K of Ω for all $t > 0$.

Thanks to 1), $C(t)$ and $q(t)$ are C^3 functions and their derivatives are uniformly bounded up to order 3 with respect to $t \geq 0$. Thanks to 1) $\psi(t,\eta)$ and $\phi(t,s)$ are C^3 functions and, thanks to 3), their derivatives are uniformly bounded up to order 3 with respect to $t \geq 0$, $\eta, s \in \mathbb{S}^2$ (use (1) and the existence of $\varsigma > 0$ with $\|\overrightarrow{C(t)M}\| \geq \varsigma$ for all $t > 0$ and $M \in \Sigma$). Thanks to 3) and (2), $y(t,\eta)$ is a C^3 function and its derivatives are uniformly bounded up to order 3 with respect to $t \geq 0$ and $\eta \in \mathbb{S}^2$. Thanks to 3), the minimum of $D(t,s) = \|\overrightarrow{C(t)M(s)}\|$ for $t \geq 0$ and $s \in \mathbb{S}^2$ is strictly positive, thus $\Gamma(t,\eta)$ is a C^3 function and its derivatives are uniformly bounded up to order 3 with respect to $t \geq 0$ and $\eta \in \mathbb{S}^2$ (see (3)). In the sequel, ∇y and $\nabla\Gamma$ denote the gradients of y and Γ on the Riemannian sphere $\mathbb{S}^2$.

B. Statement of the bias estimation problem

Under the above assumptions, the y and Γ obey to ([17], [18])

$$\dot{y} = -\nabla y \cdot (\eta \times (\omega + \Gamma\eta \times v)) \tag{4}$$

$$\dot{\Gamma} = -\nabla\Gamma \cdot (\eta \times (\omega + \Gamma\eta \times v)) + \Gamma^2 v \cdot \eta \tag{5}$$

where $\dot{y}$ and $\dot{\Gamma}$ stand for partial derivatives of y and Γ with respect to t. The Euclidean scalar product of two vectors a and b in $\mathbb{R}^3$ is denoted by $a \cdot b$ and their wedge product by $a \times b$. Equations (4) and (5) are $SO(3)$-invariant: they remain unchanged by any rotation described by the quaternion σ and changing (η, ω, v) to $(\sigma\eta\sigma^*, \sigma\omega\sigma^*, \sigma v\sigma^*)$.

The camera motion characterized by (v,ω) is not known precisely. We assume here that sensor data provide $v_m(t)$ and $\omega_m(t)$ differing from true velocities by measurement biases, defined as constant errors:

$$v_m(t) = v(t) + p_v, \quad \omega_m(t) = \omega(t) + p_\omega \tag{6}$$

where $p_v, p_\omega \in \mathbb{R}^3$ are constant:

$$\dot{p_v} = 0, \quad \dot{p_\omega} = 0 \tag{7}$$

The state equations are given by (4), (5) and (7) where $v(t)$ and $\omega(t)$ depend on the unknown parameters p_v and p_ω via (6). Here (v_m, ω_m) are considered as known inputs

and (y, Γ) as the measured outputs. The goal is to estimate in real-time the parameters (p_v, p_ω) from the known signals y, Γ, v and ω. Notice that, as assumed in the previous subsection, y and Γ are C^3 with respect to t and η with bounded partial derivatives up to order 3.

III. The asymptotic observer

A. A Lyapunov based observer

We propose the following observer for p_ω and p_v, inspired by the one proposed in [17]:

$$\left\{\begin{array}{l} \dot{\widehat{y}} = -\nabla\widehat{y}\cdot(\eta\times(\omega_m-\widehat{p_\omega}+\Gamma\eta\times(v_m-\widehat{p_v}))) \\ \qquad +k_y(y-\widehat{y}) \\ \dot{\widehat{\Gamma}} = -\nabla\widehat{\Gamma}\cdot(\eta\times(\omega_m-\widehat{p_\omega}+\Gamma\eta\times(v_m-\widehat{p_v}))) \\ \qquad +\Gamma^2(v_m-\widehat{p_v})\cdot\eta+k_\Gamma(\Gamma-\widehat{\Gamma}) \\ \dot{\widehat{p_\omega}} = -k_\omega\int_{\mathbb{S}^2}\Big(\lambda_y(\widehat{y}-y)(\nabla\widehat{y}\times\eta) \\ \qquad\qquad +\lambda_\Gamma(\widehat{\Gamma}-\Gamma)(\nabla\widehat{\Gamma}\times\eta)\Big)d\sigma_\eta \\ \dot{\widehat{p_v}} = k_v\int_{\mathbb{S}^2}\Big(\lambda_\Gamma(\widehat{\Gamma}-\Gamma)\Gamma^2\eta \\ \qquad -\lambda_y(\widehat{y}-y)(\Gamma\eta\times(\eta\times\nabla\widehat{y})) \\ \qquad -\lambda_\Gamma(\widehat{\Gamma}-\Gamma)(\Gamma\eta\times(\eta\times\nabla\widehat{\Gamma}))\Big)\,d\sigma_\eta \end{array}\right. \tag{8}$$

where k_y, k_Γ, k_ω, k_v, λ_y, λ_Γ are constant positive gains. The choice of this observer is justified by the following Lyapunov function:

$$V=\frac{1}{2}\left(\int_{\mathbb{S}^2}\left(\lambda_y\widetilde{y}^2+\lambda_\Gamma\widetilde{\Gamma}^2\right)d\sigma_\eta+\frac{\|\widetilde{p_\omega}\|^2}{k_\omega}+\frac{\|\widetilde{p_v}\|^2}{k_v}\right)$$

with $\widetilde{y}=\widehat{y}-y$, $\widetilde{\Gamma}=\widehat{\Gamma}-\Gamma$, $\widetilde{p_\omega}=\widehat{p_\omega}-p_\omega$ and $\widetilde{p_v}=\widehat{p_v}-p_v$. To prove that V decreases as the time t increases, let us consider any scalar field $h(t,\eta)$ defined on $\mathbb{S}^2$ and its integral $\mathcal{H}$ on the unit sphere:

$$\mathcal{H}=\int_{\mathbb{S}^2}h(t,\eta)^2d\sigma_\eta=\int_{\mathbb{S}^2}h(t,q^*\eta q)^2d\sigma_\eta$$

since $\eta\mapsto q^*\eta q$ is an isometry on $\mathbb{S}^2$. For η a constant vector of the earth-fixed frame, $q^*\eta q$ is the same vector, expressed in the camera frame. Thus, $h(t,q^*\eta q)$ is the value of h corresponding to a specific object $M(s)$ of the scene. This yields

$$\begin{aligned}\tfrac{d}{dt}\mathcal{H}&=\int_{\mathbb{S}^2}\tfrac{d}{dt}(h(t,q^*\eta q)^2)d\sigma_\eta\\&=2\int_{\mathbb{S}^2}h(t,q^*\eta q)\ \tfrac{d}{dt}h(t,q^*\eta q)\big|_s\,d\sigma_\eta\\&=2\int_{\mathbb{S}^2}h(t,q^*\eta q)\left(\dot{h}+\nabla h\cdot(\eta\times(\omega+\Gamma\eta\times v))\right)d\sigma_\eta\end{aligned}$$

One can apply this calculation rule to the scalar fields $\widetilde{y}$ and $\widetilde{\Gamma}$. Then, (4) and (8) yield

$$\begin{aligned}\dot{\widetilde{y}}+\nabla\widetilde{y}\cdot(\eta\times(\omega+\Gamma\eta\times v))\\=\nabla\widehat{y}\cdot(\eta\times(\widetilde{p_\omega}+\Gamma\eta\times\widetilde{p_v}))-k_y\widetilde{y}.\end{aligned}\tag{9}$$

Equations (5) and (8) yield

$$\begin{aligned}\dot{\widetilde{\Gamma}}+\nabla\widetilde{\Gamma}\cdot(\eta\times(\omega+\Gamma\eta\times v))\\=\nabla\widehat{\Gamma}\cdot(\eta\times(\widetilde{p_\omega}+\Gamma\eta\times\widetilde{p_v}))-\Gamma^2\eta\cdot\widetilde{p_v}-k_\Gamma\widetilde{\Gamma}.\end{aligned}\tag{10}$$

Now, using $a\cdot(b\times c)=(a\times b)\cdot c$ and the expressions of $\dot{\widehat{p_\omega}}$ and $\dot{\widehat{p_v}}$, one finally gets

$$\dot{V}=-\int_{\mathbb{S}^2}\left(k_y\lambda_y\widetilde{y}^2+k_\Gamma\lambda_\Gamma\widetilde{\Gamma}^2\right)d\sigma_\eta.$$

The Lyapunov function V decreases along the trajectories. The convergence analysis will be done by proving, under the assumptions given in subsection II-A, the following successive steps:

1) the non-linear partial differential equations (8) define a well posed Cauchy problem for $t\geq 0$ as soon as the initial state $\widehat{y}$ and $\widehat{\Gamma}$ are C^3 versus t and η; moreover the partial derivatives of $\widehat{y}$, $\widehat{\Gamma}$, $\widehat{p_v}$ and $\widehat{p_\omega}$ up to order 3 are uniformly bounded with respect to $t\geq 0$ and $\eta\in\mathbb{S}^2$.
2) since $t\mapsto\dot{V}$ is proved to converge to zero as t tends to infinite, the estimates $\widehat{y}$ and $\widehat{\Gamma}$ tend to y and Γ; since partial derivatives of order 3 are bounded uniformly with respect to t, such convergence occurs also for C^1-norm topology; its yields to a geometric characterization (depending only on the shape of the domain Ω) of the possible limit set for $\widetilde{p_v}$ and $\widetilde{p_\omega}$.
3) we conjecture that this geometric characterization is reduced to $\widetilde{p_v}=\widetilde{p_\omega}=0$ when the convex domain $\Omega\subset\mathbb{R}^3$ inside which the camera moves admits no rotational symmetry axis.

B. Well posedness and bounds for the observer

Existence and uniqueness of solutions of (8) is given by the next statement.

Theorem 1: Assume that

$$[0,+\infty[\times\mathbb{S}^2\ni(t,\eta)\mapsto(y(t,\eta),\Gamma(t,\eta),v(t),\omega(t))$$

obeying to (4), (5) satisfy the regularity assumptions of subsection II-A. Then for every $(\widehat{y}_0,\widehat{\Gamma}_0,\widehat{p_v}_0,\widehat{p_\omega}_0)\in C^3(\mathbb{S}^2,\mathbb{R})^2\times\mathbb{R}^6$, there exists a unique solution $(\widehat{y},\widehat{\Gamma},\widehat{p_v},\widehat{p_\omega})\in C^3([0,+\infty)\times\mathbb{S}^2,\mathbb{R})^2\times C^3([0,+\infty),\mathbb{R}^3)^2$ of (8) such that

$$\begin{aligned}\forall\eta\in\mathbb{S}^2,\quad(\widehat{y}(0,\eta),\widehat{\Gamma}(0,\eta),\widehat{p_v}(0),\widehat{p_\omega}(0))\\=(\widehat{y}_0(\eta),\widehat{\Gamma}_0(\eta),\widehat{p_v}_0,\widehat{p_\omega}_0).\end{aligned}$$

Moreover, all partial derivatives versus t and η, up to order 3, of $\widehat{y}$, $\widehat{\Gamma}$, $\widehat{p_v}$, $\widehat{p_\omega}$ are uniformly bounded with respect to $t\geq 0$ and $\eta\in\mathbb{S}^2$.

Proof: In a first step, let us assume that $(\widehat{y},\widehat{\Gamma},\widehat{p_v},\widehat{p_\omega})$ is a solution. Let $\varphi=\varphi(t,\eta)$ be the characteristics

$$\left\{\begin{array}{l}\dot{\varphi}=\varphi\times(\omega-\widehat{p_\omega}+\Gamma(t,\varphi)\varphi\times(v-\widehat{p_v})),\\ \varphi(0,\eta)=\eta.\end{array}\right.\tag{11}$$

The functions $\hat{h}(t,\eta)=\widehat{\Gamma}(t,\varphi(t,\eta))$, $\hat{k}(t,\eta)=\widehat{y}(t,\varphi(t,\eta))$ solve

$$\left\{\begin{array}{l}\dot{\hat{h}}=h^2(v-\widehat{p_v}).\varphi+k_\Gamma(h-\hat{h}),\\ \hat{h}(0,\eta)=\widehat{\Gamma}_0(\eta),\end{array}\right.\qquad\left\{\begin{array}{l}\dot{\hat{k}}=k_y(k-\hat{k}),\\ \hat{k}(0,\eta)=\widehat{y}_0(\eta).\end{array}\right.$$

where $h(t,\eta) = \Gamma(t,\varphi(t,\eta))$ and $k(t,\eta) = y(t,\varphi(t,\eta))$. Thus $\widehat{y}$ and $\widehat{\Gamma}$ satisfy

$$\widehat{y}(t,\varphi(t,\eta)) = \widehat{y}_0(\eta)e^{-k_y t} + \int_0^t k_y y(\tau,\varphi(\tau,\eta))e^{k_y(\tau-t)}d\tau \quad (12)$$

and

$$\widehat{\Gamma}(t,\varphi(t,\eta)) = \widehat{\Gamma}_0(\eta)e^{-k_\Gamma t} + \int_0^t \Big[\Gamma^2(\tau,\varphi(\tau,\eta))(v(\tau) - \widetilde{p_v}(\tau)) + k_\Gamma \Gamma(\tau,\varphi(\tau,\eta))\Big]e^{k_\Gamma(\tau-t)}d\tau. \quad (13)$$

Thus, the characteristic equations (11) are nonlinear integro-differential equations. Indeed, $\widehat{p_v}(t)$ may be replaced by

$$\widehat{p_v}(t) = \widehat{p_v}_0 + \int_0^t \frac{d\widehat{p_v}}{d\tau}(\tau)d\tau,$$

where $\frac{d\widehat{p_v}}{d\tau}$ may be replaced by its expression given in (8), in which $\widehat{y}$ and $\widehat{\Gamma}$ may be replaced by (12) and (13) (idem for $\widehat{p_\omega}$). The existence and uniqueness of local solutions may be proved with a fixed point argument. Maximal solutions are global because there is no explosion in finite time. This ends the proof of the well posedness.

To prove that $\widehat{y}$, $\widehat{\Gamma}$ $\widetilde{p_v}$ and $\widetilde{p_\omega}$ and their partial derivatives versus t and η up to order 3 are uniformly bounded with respect to $t > 0$ and $\eta \in \mathbb{S}^2$, let us state the following lemma (proven in appendix).

Lemma 1: Consider the following partial differential equation:

$$\dot{h} = \frac{\partial h}{\partial \eta}\cdot F(t,\eta) + a(t,\eta)h + G(t,\eta) - kh$$

where $h : (t,\eta) \in [0,+\infty)\times\mathbb{S}^2 \to \mathbb{R}$ and k is a positive constant. Let $n \in \mathbb{N}^*$. Assuming that the partial derivatives up-to order n of F, a and G with respect to t and η are uniformly bounded, then $\exists\, k^*$ such that $\forall k \geq k^*$, the partial derivatives up-to order n of h with respect to t and η are uniformly bounded.

Now, let us prove the uniform bounds of Proposition 1. Lemma 1 applies to $\widehat{y}$ with

- $F(t,\eta) = -\eta\times(\omega - \widetilde{p_\omega} + \Gamma\eta\times(v - \widetilde{p_v}))$
- $a(t,\eta) = 0$
- $G(t,\eta) = k_y y(t,\eta)$

Indeed, as V is a Lyapunov function (therefore bounded), there exists a constant $V_M > 0$ such that, $\forall t \geq 0$,

$$\int_{\mathbb{S}^2}\widetilde{y}^2, \quad \int_{\mathbb{S}^2}\widetilde{\Gamma}^2, \quad \|\widetilde{p_v}\|, \quad \|\widetilde{p_\omega}\| \leqslant V_M \quad (14)$$

and F, G and their partial derivatives with respect to η are uniformly bounded. Thus $\widehat{y}$ and $\nabla\widehat{y}$ are uniformly bounded. Similarly, Lemma 1 applies to $\widehat{\Gamma}$. Then, we get from (8) that the time-derivatives of $\widetilde{p_v}$ and $\widetilde{p_\omega}$ are uniformly bounded. The same reasoning applies to prove the uniform boundedness up to order 3. ∎

C. The Ω-limit set

Theorem 2: Under the assumptions of theorem 1 we have

1) - $\lim_{t\to+\infty}\sup_{\eta\in\mathbb{S}^2}|\widetilde{y}| + \|\nabla\widetilde{y}\| + |\dot{\widetilde{y}}| = 0$
   - $\lim_{t\to+\infty}\sup_{\eta\in\mathbb{S}^2}|\widetilde{\Gamma}| + \|\nabla\widetilde{\Gamma}\| + |\dot{\widetilde{\Gamma}}| = 0$
2) for every adherence value (P_v, P_ω) of $(\widetilde{p_v}, \widetilde{p_\omega})$ as $t\to+\infty$, there exists $\bar{C}\in K\subset\Omega$ a camera position such that, $\forall\eta\in\mathbb{S}^2$

$$(\nabla\bar{y}\times\eta)\cdot P_\omega + \bar{\Gamma}\eta\times(\eta\times\nabla\bar{y})\cdot P_v = 0 \quad (15)$$

$$(\nabla\bar{\Gamma}\times\eta)\cdot P_\omega - (\bar{\Gamma}^2\eta - \bar{\Gamma}\eta\times(\eta\times\nabla\bar{\Gamma}))\cdot P_v = 0 \quad (16)$$

where $\bar{y}(t,\eta)$ and $\bar{\Gamma}(t,\eta)$ are the brightness and depth fields associated to the position $\bar{C}$ of the camera with orientation $\bar{q} = 1$.

Proof: In a first step we prove that

$$f(t) := \frac{1}{2}\int_{\mathbb{S}^2} k_y\widetilde{y}^2 + k_\Gamma\widetilde{\Gamma}^2 d\sigma_\eta$$

converges to zero as $t\to+\infty$. Note that $\dot{V} = -f(t)$ and V converges as $t\to+\infty$ (because non increasing and $\geqslant 0$). Thus $f\in L^1(0,+\infty)$. In order to conclude, it is sufficient to prove that f is uniformly continuous on $[0,+\infty)$ (Barbalat Lemma). We have

$$\dot{f} = \int_{\mathbb{S}^2}\Big(k_y\widetilde{y}(\nabla\widehat{y}\cdot(\eta\times(\widetilde{p_\omega} + \Gamma\eta\times\widetilde{p_v})) - k_y\widetilde{y}) + k_\Gamma\widetilde{\Gamma}(\nabla\widehat{\Gamma}\cdot(\eta\times(\widetilde{p_\omega} + \Gamma\eta\times\widetilde{p_v})) + \Gamma^2\eta\cdot\widetilde{p_v} - k_\Gamma\widetilde{\Gamma})\Big)d\sigma_\eta$$

Under assumptions described in II-A, Proposition 1 proves that $\nabla\widehat{y}$, $\nabla\widehat{\Gamma}$ are uniformly bounded with respect to $t\geqslant 0$ and $\eta\in\mathbb{S}^2$. Thanks to Cauchy-Schwarz inequality, $\dot{f}(t)$ is bounded uniformly with respect to $t\geqslant 0$, which ends the proof of the first step.

Second step: let us prove the first conclusion of the theorem. Under assumptions described in II-A, theorem 1 proves that $\widetilde{y}$, $\widetilde{\Gamma}$ and their partial derivatives up to order 3 are uniformly bounded with respect to $t\geqslant 0$ and $\eta\in\mathbb{S}^2$. Thus partial derivatives up to second order admit, according to Ascoli-Arzela theorem, accumulation η-functions when t tends to $+\infty$. Let us consider such accumulation functions, $\overline{\widetilde{y}}$, $\overline{\widetilde{\Gamma}}$, $\overline{\nabla\widetilde{y}}$, $\overline{\nabla\widetilde{\Gamma}}$, $\overline{\dot{\widetilde{y}}}$, $\overline{\dot{\widetilde{\Gamma}}}$ for $\widetilde{y}$, $\widetilde{\Gamma}$, $\nabla\widetilde{y}$, $\nabla\widetilde{\Gamma}$, $\dot{\widetilde{y}}$, $\dot{\widetilde{\Gamma}}$ respectively. Thus exists $(t_n)\in[0,+\infty)^{\mathbb{N}}$ with $t_n\to+\infty$ such that $\widetilde{y}(t_n)\to\overline{\widetilde{y}}$, $\widetilde{\Gamma}(t_n)\to\overline{\widetilde{\Gamma}}$, $\nabla\widetilde{y}(t_n)\to\overline{\nabla\widetilde{y}}$, $\nabla\widetilde{\Gamma}(t_n)\to\overline{\nabla\widetilde{\Gamma}}$, $\dot{\widetilde{y}}(t_n)\to\overline{\dot{\widetilde{y}}}$ and $\dot{\widetilde{\Gamma}}(t_n)\to\overline{\dot{\widetilde{\Gamma}}}$ where $\to$ stands for convergence with the L_∞-norm on $\eta\in\mathbb{S}^2$. Such uniforme convergence yields $\overline{\nabla\widetilde{y}} = \nabla\overline{\widetilde{y}}$ and $\overline{\nabla\widetilde{\Gamma}} = \nabla\overline{\widetilde{\Gamma}}$. According to the first step of this proof, the only possible value for $(\overline{\widetilde{y}}, \overline{\widetilde{\Gamma}})$ is $(0,0)$ and thus $(\overline{\nabla\widetilde{y}}, \overline{\nabla\widetilde{\Gamma}})$=$(0,0)$. Now, considering the time-derivatives of f, one gets:

$$\dot{f} = 2\int_{\mathbb{S}^2}\left(k_y\widetilde{y}\dot{\widetilde{y}} + k_\Gamma\widetilde{\Gamma}\dot{\widetilde{\Gamma}}\right)d\sigma_\eta$$

$$\ddot{f} = 2\int_{\mathbb{S}^2}\left(k_y(\widetilde{y}\ddot{\widetilde{y}} + \dot{\widetilde{y}}^2) + k_\Gamma(\widetilde{\Gamma}\ddot{\widetilde{\Gamma}} + \dot{\widetilde{\Gamma}}^2)\right)d\sigma_\eta$$

Thus, $\dot{f}(t_n)$ tends to 0 and $\ddot{f}(t_n)$ tends to

$$2\int_{\mathbb{S}^2}\left(k_y\left(\dot{\widetilde{y}}\right)^2+k_\Gamma\left(\dot{\widetilde{\Gamma}}\right)^2\right)d\sigma_\eta.$$

Moreover $\ddot{f}$ is uniformly continuous ($f^{(3)}$ is uniformly bounded because $\widetilde{y}$ and $\widetilde{\Gamma}$ are bounded in C^3 topology), this yields $\dot{\widetilde{f}}(t_n)\to 0$ as $n\to+\infty$ and thus $\dot{\widetilde{y}}(t_n)\to 0$ and $\dot{\widetilde{\Gamma}}(t_n)\to 0$. This proves the first conclusion of theorem 2.

Third step: Let us prove the second conclusion of the theorem. Combining (4), (5) and (8) with the convergence of $\widetilde{y}$ and $\widetilde{\Gamma}$ towards 0 for C^1 topology yields, $\forall\eta\in\mathbb{S}^2$:

$$\lim_{t\to+\infty}(\nabla y\times\eta)\cdot\widetilde{p_\omega}+\Gamma\eta\times(\eta\times\nabla y)\cdot\widetilde{p_v}=0,$$
$$\lim_{t\to+\infty}(\nabla\Gamma\times\eta)\cdot\widetilde{p_\omega}-(\Gamma^2\eta-\Gamma\eta\times(\eta\times\nabla\Gamma))\cdot\widetilde{p_v}=0.$$

Let us consider accumulation points $\overline{y}$, $\overline{\Gamma}$, $\overline{\widetilde{p_v}}$ and $\overline{\widetilde{p_\omega}}$ of y, Γ, $\widetilde{p_v}$ and $\widetilde{p_\omega}$ for t tending to $+\infty$ (Ascoli-Arzela theorem for y and Γ and $\widetilde{p_v}$, $\widetilde{p_\omega}$ bounded). According to subsection II-A, $\overline{y}$ and $\overline{\Gamma}$ correspond to accumulation points $\overline{C}$ and $\overline{q}$ for $C(t)$ and $q(t)$. The above two limits provide, for all $\eta\in\mathbb{S}^2$,

$$(\nabla\overline{y}\times\eta)\cdot\overline{\widetilde{p_\omega}}+\overline{\Gamma}\eta\times(\eta\times\nabla\overline{y})\cdot\overline{\widetilde{p_v}}=0,$$
$$(\nabla\overline{\Gamma}\times\eta)\cdot\overline{\widetilde{p_\omega}}-(\overline{\Gamma}^2\eta-\overline{\Gamma}\eta\times(\eta\times\nabla\overline{\Gamma}))\cdot\overline{\widetilde{p_v}}=0.$$

Since these equations are $SO(3)$-invariant, we can set $\bar{q}=1$ and we recover (15) and (16). ∎

D. Characterization of the invariant set

We have seen in sub-section III-C that the possible accumulation points P_v and P_ω for $\widetilde{p_v}$ and $\widetilde{p_\omega}$ satisfy the constraint

$$(\nabla\overline{\Gamma}\times\eta)\cdot P_\omega-(\overline{\Gamma}^2\eta-\overline{\Gamma}\eta\times(\eta\times\nabla\overline{\Gamma}))\cdot P_v=0$$

where $\overline{\Gamma}$ is the depth profile associated to a position $\overline{C}$ inside the domain Ω and with orientation $\bar{q}=1$. We conjecture that, if the convex domain $\Omega\subset\mathbb{R}^3$ does not admit any rotational symmetry axis, such constraint is only satisfied for $P_v=P_\omega=0$. This conjecture leans on the following elementary geometric properties:

- for $P_v=0$, this constraint becomes $\nabla\overline{\Gamma}\cdot(\eta\times P_\omega)=0$, which characterizes a rotational symmetry of Σ around the $(\overline{C},P_\omega)$ axis;
- for $P_\omega=0$, $(\overline{\Gamma}^2\eta-\overline{\Gamma}\eta\times(\eta\times\nabla\overline{\Gamma}))\cdot P_v=0$ cannot be satisfied for $P_v\neq 0$ since for η colinear to P_v, we get $\overline{\Gamma}\|P_v\|=0$ ($\overline{\Gamma}$ is always >0).

IV. Practical implementation and simulations

A. Adaptation to a spherical cap

Concretely, a spherical camera is only a model, and the image perceived by real cameras only occupy a part of $\mathbb{S}^2$. Let us call K this portion: $y(t,\eta)$ and $\Gamma(t,\eta)$ are known only for $\eta\in K$. The observer introduced in III can not be readily used since it brings into play the integral of y or Γ over the whole unit sphere. We will see that one can compensate this problem by considering virtual observations, equal to the real observations over the window defined by K. Let K_1 and K_2 be two compact sets s.t. $\overset{\circ}{K_1}\subset\overset{\circ}{K_2}\subset\overset{\circ}{K}$. Let be a $\mathcal{C}^\infty$ scalar field $\mathbb{S}^2\ni\eta\mapsto\phi(\eta)\in\mathbb{R}$, s.t. $\phi=1$ on K_1, $\phi=0$ on $\mathbb{S}^2\setminus K_2$. Let us define $Y=\phi y$ and $\Lambda=\phi\Gamma$. Then,

$$\dot{Y}=-\nabla Y\cdot(\eta\times(\omega+\Gamma\eta\times v))+y\nabla\phi\cdot(\eta\times(\omega+\Gamma\eta\times v))$$

and

$$\dot{\Lambda}=-\nabla\Lambda\cdot(\eta\times(\omega+\Gamma\eta\times v))+\Gamma\nabla\phi\cdot(\eta\times(\omega+\Gamma\eta\times v))+\Gamma\Lambda\eta\cdot v.$$

The adaptation of observer (8) reads

$$\begin{aligned}
\dot{\widehat{Y}}=\;&-\nabla\widehat{Y}\cdot(\eta\times(\omega_m-\widehat{p_\omega}+\Gamma\eta\times(v_m-\widehat{p_v})))\\
&+y\nabla\phi\cdot(\eta\times(\omega_m-\widehat{p_\omega}+\Gamma\eta\times(v_m-\widehat{p_v})))\\
&+k_Y(Y-\widehat{Y})\\
\dot{\widehat{\Lambda}}=\;&-\nabla\widehat{\Lambda}\cdot(\eta\times(\omega_m-\widehat{p_\omega}+\Gamma\eta\times(v_m-\widehat{p_v})))\\
&+\Gamma\nabla\phi\cdot(\eta\times(\omega_m-\widehat{p_\omega}+\Gamma\eta\times(v_m-\widehat{p_v})))\\
&+\Gamma\Lambda(v_m-\widehat{p_v})\cdot\eta+k_\Lambda(\Lambda-\widehat{\Lambda})\\
\dot{\widehat{p_\omega}}=\;&-k_\omega\textstyle\int_K\lambda_Y(\widehat{Y}-Y)((\nabla\widehat{Y}-y\nabla\phi)\times\eta)\\
&+\lambda_\Lambda(\widehat{\Lambda}-\Lambda)((\nabla\widehat{\Lambda}-\Gamma\nabla\phi)\times\eta)d\sigma_\eta\\
\dot{\widehat{p_v}}=\;&k_v\textstyle\int_K\lambda_\Lambda(\widehat{\Gamma}-\Gamma)\Gamma\Lambda\eta\\
&-\lambda_Y(\widehat{Y}-Y)(\Gamma\eta\times(\eta\times(\nabla\widehat{Y}-y\nabla\phi))\\
&-\lambda_\Lambda(\widehat{\Lambda}-\Lambda)(\Gamma\eta\times(\eta\times(\nabla\widehat{\Lambda}-\Gamma\nabla\phi))d\sigma_\eta
\end{aligned}\tag{17}$$

Integrals on $\mathbb{S}^2$ are actually integrals on K since the integrands vanish out of K. Let us choose the Lyapunov function

$$V=\frac{1}{2}\left(\int_K\left(\lambda_Y(\widehat{Y}-Y)^2+\lambda_\Lambda(\widehat{\Lambda}-\Lambda)^2\right)d\sigma_\eta+\frac{(\widehat{p_\omega}-p_\omega)^2}{k_\omega}+\frac{(\widehat{p_v}-p_v)^2}{k_v}\right).$$

One can prove just as previously that

$$\dot{V}=\int_K\left(-\lambda_Y k_Y(\widehat{Y}-Y)^2-\lambda_\Lambda k_\Lambda(\widehat{\Lambda}-\Lambda)^2\right)d\sigma_\eta.$$

We guess that convergence analysis done when $K=\mathbb{S}^2$ can be extended to compact sub-domains K of $\mathbb{S}^2$.

B. The observer in pinhole coordinates

The previous observer can be finally adapted to a real model of camera: the widely spread pinhole camera model enabling a correspondence between the local coordinates on $\mathbb{S}^2$ with a rectangular grid of pixels. The pixel of coordinates (z_1,z_2) corresponds to the unit vector $\eta\in\mathbb{S}^2$ of coordinates in $\mathbb{R}^3$: $\left(1+z_1^2+z_2^2\right)^{-1/2}(z_1,z_2,1)^T$. The optical camera axis (pixel $(z_1,z_2)=(0,0)$) corresponds here to the direction z_3. Directions 1 and 2 correspond respectively to the horizontal axis from left to right and to the vertical axis from top to bottom on the image frame.

The gradients ∇y and $\nabla\Gamma$ must be expressed with respect to z_1 and z_2. Let us detail this derivation for y. Firstly, ∇y is tangent to $\mathbb{S}^2$, thus $\nabla y\cdot\eta=0$. Secondly, the differential dy corresponds to $\nabla y\cdot d\eta$ and to $\frac{\partial y}{\partial z_1}dz_1+\frac{\partial y}{\partial z_2}dz_2$. By identification, we get the Cartesian coordinates of ∇y in $\mathbb{R}^3$. Similarly we get the three coordinates of $\nabla\Gamma$. Injecting these expressions in (17), we get a partial differential equations

(PDE) system written in terms of (t, z_1, z_2) as independent variables. Due to space limitation, this system is not given here, but its derivation is straightforward and a little bit tedious.

C. Simulations

The non-linear asymptotic observer (17) is tested on a sequence of synthetic images characterized by the following:

- *virtual camera*: the size of each image is 640 by 480 pixels, the frame rate of the sequence is 42 Hz and the field of view is 50 deg by 40 deg (defining K).
- *motion of the virtual camera*: it consists of the motion of a real hand-held camera (filtered data), combining translations and rotations in each direction; the real linear and angular velocities expressed in the camera frame are plotted in Fig.2 and Fig.3; zero-mean normally distributed noise (standard deviations σ_v and σ_ω) is added to these velocities to test the robustness;
- *virtual scene*: it consists of the walls, ceiling and floor of a virtual room; the observed walls are virtually painted with a gray pattern, whose intensity varies in horizontal and vertical directions as a sinusoid function;
- *generation of the images*: each pixel of an image has an integer value varying from 1 to 256, directly depending on the intensity of the observed surface in the direction indexed by the pixel, to which a zero-mean normally distributed noise with standard deviation σ_y is added to test the robustness;
- *generation of the depth images*: to each pixel of the rectangular grid of an image is attributed the depth of the corresponding element of the observed surface, computed with respect with position and orientation of the camera in the room, to which a zero-mean normally distributed noise with standard deviation σ_D is added to test the robustness.

The numerical resolution used to compute $\widehat{y}$, $\widehat{\Gamma}$, $\widehat{p_\omega}$ and $\widehat{p_v}$ according to (8) is based on a temporal Euler discretization scheme where $\nabla\widehat{y}$ and $\nabla\widehat{\Gamma}$ are computed via differentiation filters (Sobel filtering) directly from the image and depth previous estimates. The observer is then tested for reasonable biases: in rotation, a bias of 0.05 rad.s^{-1} ($10,000$ deg/h, for a low-cost gyroscope) around the horizontal axis; in translation, a bias of 2.5 m.s^{-1} in the horizontal direction (9 km/h, for the windspeed). In other words, $p_{\omega_1} = 0.05$ rad.s^{-1} and $p_{v_x} = 2.5$ m.s^{-1}. Biases in the other directions are set to 0. Initial conditions for $\widehat{y}$ and $\widehat{\Gamma}$ are $y(0,\eta)$ and $\Gamma(0,\eta)$. Initial conditions for the estimated biases are set to zero. The chosen correction gains are: $k_y = k_\Gamma = 2s^{-1}$, $k_v = 10^{-2}\text{m}^2.s^{-2}$ and $k_\omega = 10^{-5}$rad.m.s^{-2}. These correction gains are chosen in accordance with the expected values of biases and the environment averaged depth, to enable a reasonable convergence speed. The correction gains k_y and k_Γ are comparatively much larger than k_v, which is itself larger than k_ω, as large oscillations in the estimation of p_ω can make the discretized observer to diverge. Finally, the ponderation coefficients are $\lambda_y = 1$ and $\lambda_\Gamma = 5000\text{m}^2$, chosen to compensate the difference of magnitudes of y and Γ. First, when image and depth data contain no noise ($\sigma_y = \sigma_D = 0$), the results are plotted in Fig.4 and Fig.5 as the instantaneous errors of estimations $\widetilde{p_v}$ and $\widetilde{p_\omega}$ expressed in the camera frame, respectively. In the first 6 s, errors slowly converge towards 0, and coupling between rotation and translation occurs: this reflects the fact that an horizontal translation can be interpreted as a rotation around the vertical axis to a certain extent. Oscillations decrease, and after convergence, errors stay bounded: for the bias in rotation, it does not exceed 0.002 rad.s^{-1} (4 % of the original bias); in translation, it is less than 0.01 m.s^{-1} (0.4 % of the original bias).

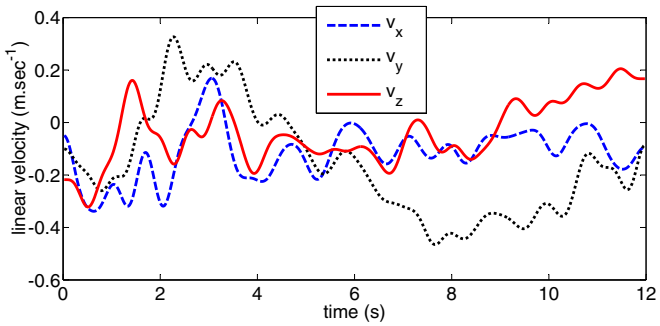

Fig. 2. Components of the linear velocity used to test the observer: translations in the horizontal, vertical and optical axis directions, respectively.

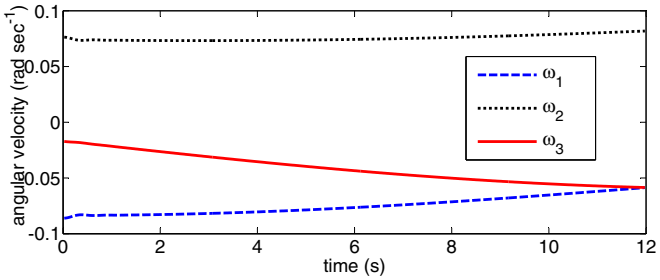

Fig. 3. Components of the angular velocity used to test the observer: rotations around the horizontal, vertical and optical axis, respectively.

Then, to test the robustness of the method, noise is added to the image data ($\sigma_y = 30$, about 12% of the full scale), to the depth data ($\sigma_D = 25$ cm, which is three times as much that can be expected from a Kinect device), to linear velocity ($\sigma_v = 0.05\text{m}.s^{-1}$) and to angular velocity ($\sigma_\omega = 0.005$ rad.s^{-1}). Results are plotted in Fig.6 and Fig.7. Convergence time is shorter for biases in translation estimation: after 3 s, error does not exceed 0.2 m.s^{-1} (8 % of the original bias). For the rotation, convergence is slower (as k_ω is smaller), but in the last 3 sec of the simulation, biases are estimated up to 0.003 rad.s^{-1} (6 % of the original bias).

V. Conclusion

We have proposed a new infinite dimensional nonlinear observer that simultaneously filters image and depth data and estimates constant biases on angular and translational velocities. Observer design is based on a Lyapunov func-

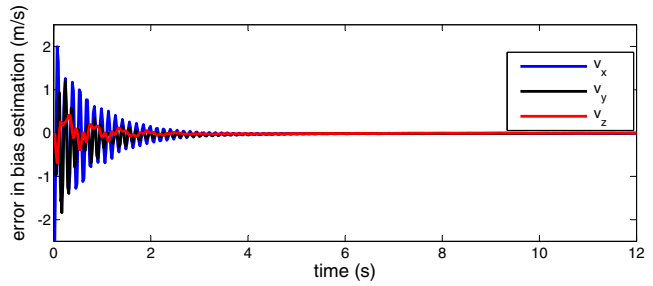

Fig. 4. Error of estimation of the biases in translation for noiseless image and depth data. Real biases are $p_{\omega_1} = 0.05$ rad.s^{-1} and $p_{v_x} = 2.5$ m.s^{-1}

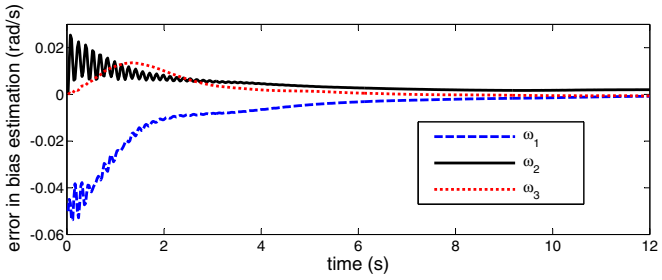

Fig. 5. Error of estimation of the biases in rotation for noiseless image and depth data. Real biases are $p_{\omega_1} = 0.05$ rad.s^{-1} and $p_{v_x} = 2.5$ m.s^{-1}

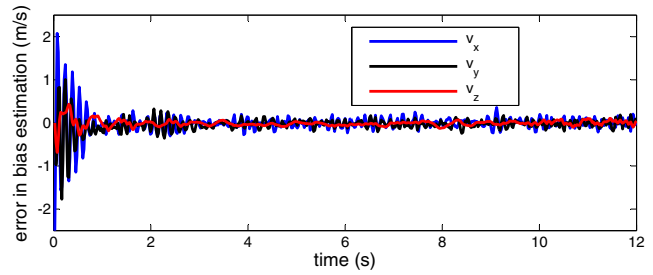

Fig. 6. Error of estimation of the biases in translation for noisy image and depth data, and noisy velocities: $\sigma_y = 30$, $\sigma_D = 25$ cm, $\sigma_v = 0.05$m.s^{-1}, $\sigma_\omega = 0.005$ rad.s^{-1}. Real biases are $p_{\omega_1} = 0.05$ rad.s^{-1} and $p_{v_x} = 2.5$ m.s^{-1}

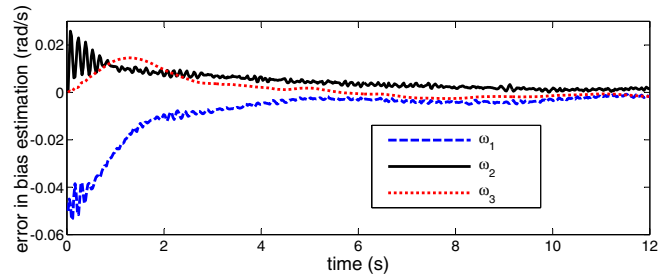

Fig. 7. Error of estimation of the biases in rotation for noisy image and depth data, and noisy velocities: $\sigma_y = 30$, $\sigma_D = 25$ cm, $\sigma_v = 0.05$m.s^{-1}, $\sigma_\omega = 0.005$ rad.s^{-1}. Real biases are $p_{\omega_1} = 0.05$ rad.s^{-1} and $p_{v_x} = 2.5$ m.s^{-1}

tional and convergence analysis has been done under C^3 regularity assumptions. We conjecture that, if the domain Ω and its boundary Σ do not admit any rotational symmetry axis, conditions (15) and (16) given in theorem 2 induce convergence of the estimated biases (estimated fields always converge). Preliminary simulations indicate that our convergence analysis could certainly be extended to more general situations with weaker regularities. It will be interesting to test the nonlinear observer (17) on real data, since Kinect-like devices can provide the necessary image and depth dense fields.

VI. Appendix 1: Proof of Lemma 1

In a first step, let us prove Lemma 1 with $a = 0$ and $n = 1$. Let us consider the solution $\varphi(t,\eta)$ to the following Cauchy problem:

$$\left\{ \begin{array}{l} \dot{\varphi} = -F(t,\varphi) \\ \varphi(0,\eta) = \eta. \end{array} \right. \tag{18}$$

The new function: $z(t,\eta) = h(t,\varphi(t,\eta))$ solves $\dot{z}(t,\eta) = G(t,\varphi(t,\eta)) - kz$. Thus

$$z(t,\eta) = e^{-kt} h_0(\eta) + \int_0^t G(\tau,\varphi(\tau,\eta)) e^{k(\tau-t)} d\tau$$

and

$$\begin{aligned} \frac{\partial z}{\partial \eta}(t,\eta) =& e^{-kt} \frac{\partial h_0}{\partial \eta}(\eta) \\ &+ \int_0^t e^{k(\tau-t)} \frac{\partial G}{\partial \eta}(\tau,\varphi(\tau,\eta)) \cdot \frac{\partial \varphi}{\partial \eta}(\tau,\eta) d\tau \end{aligned}$$

On the other hand, $\frac{\partial z}{\partial \eta}(t,\eta) = \frac{\partial h}{\partial \eta}(t,\varphi(t,\eta)) \cdot \frac{\partial \varphi}{\partial \eta}(t,\eta)$ yields

$$\begin{aligned} &\frac{\partial h}{\partial \eta}(t,\varphi(t,\eta)) = e^{-kt} \frac{\partial h_0}{\partial \eta}(\eta) \left(\frac{\partial \varphi}{\partial \eta}(t,\eta) \right)^{-1} \\ &+ \int_0^t e^{k(\tau-t)} \frac{\partial G}{\partial \eta}(\tau,\varphi(\tau,\eta)) \cdot \frac{\partial \varphi}{\partial \eta}(\tau,\eta) \cdot \left(\frac{\partial \varphi}{\partial \eta}(t,\eta) \right)^{-1} d\tau \end{aligned}$$

Considering the function

$$\Sigma(\tau,t,\eta) = \frac{\partial \varphi}{\partial \eta}(\tau,\eta) \cdot \left(\frac{\partial \varphi}{\partial \eta}(t,\eta) \right)^{-1}$$

yields

$$\left\{ \begin{array}{ll} \frac{\partial \Sigma}{\partial \tau} & = \frac{\partial}{\partial \tau}(\frac{\partial \varphi}{\partial \eta})(\tau,\eta) \cdot \left(\frac{\partial \varphi}{\partial \eta}(t,\eta) \right)^{-1} \\ & = -\frac{\partial F}{\partial \eta}(\tau,\varphi(\tau,\eta))\Sigma \\ \Sigma(t,t,\eta) & = Id \end{array} \right.$$

Since $\frac{\partial F}{\partial \eta}$ is uniformly bounded (let us denote M_1 this bound), this implies that $\exists \alpha > 0$ s.t. $\forall t,\tau \geq 0$, $||\Sigma(\tau,t,\eta)|| \leq \alpha e^{M_1|t-\tau|}$. Then, from (18), φ satisfies $\frac{\partial}{\partial t}(\frac{\partial \varphi}{\partial \eta}) = -\frac{\partial F}{\partial \eta}\frac{\partial \varphi}{\partial \eta}$. Thus

$$\frac{\partial}{\partial t} \left(\frac{\partial \varphi}{\partial \eta}(t,\eta) \right)^{-1} = \left(\frac{\partial \varphi}{\partial \eta}(t,\eta) \right)^{-1} \frac{\partial F}{\partial \eta}(t,\varphi(t,\eta))$$

and $|| \left(\frac{\partial \varphi}{\partial \eta}(t,\eta) \right)^{-1} || \leq \beta e^{M_1 t}$ for some constant $\beta > 0$. Finally, using $||\frac{\partial G}{\partial \eta}|| \leq M_2$

$$\begin{aligned} ||\frac{\partial h}{\partial \eta}(t,\varphi(t,\eta))|| &\leq e^{-kt}||\frac{\partial h_0}{\partial \eta}(\eta)||\beta e^{M_1 t} \\ &\quad + \int_0^t e^{k(\tau-t)} M_2 \alpha e^{M_1(t-\tau)} d\tau \\ &\leq \beta\delta + \frac{M_2 \alpha}{k - M_1} \end{aligned}$$

for some constant $\delta > 0$, which proves that h and $\frac{\partial h}{\partial \eta}$ are uniformly bounded, when $k > M_1$. This ends the proof of Lemma 1 with $a = 0$ and $n = 1$.

The proof with $a \neq 0$ and $n = 1$ may be done similarly: '$-kt$' is replaced by '$-kt + \int_0^t a(s, \varphi(s,\eta))$' in the exponential and k^* has to be large regarding M_1 and a). The proof with $n \in \mathbb{N}$ follows by induction on n.

REFERENCES

[1] S. M. Bezick, A. J. Pue, and C. M. Patzelt, "Inertial navigation for guided missile systems," *Johns Hopkins APL technical digest*, vol. 28, pp. 331–342, 2010.

[2] E. Abbott and D. Powell, "Land-vehicle navigation using GPS," *Proceedings of the IEEE*, vol. 87, no. 1, pp. 145–162, 1999.

[3] I. Skog and P. Handel, "In-car positioning and navigation technologies; a survey," *Intelligent Transportation Systems, IEEE Transactions on*, vol. 10, no. 1, pp. 4 –21, march 2009.

[4] D. Vissière, A. Martin, and N. Petit, "Using spatially distributed magnetometers to increase IMU-based velocity estimation in perturbed areas," in *Proc. of the* 46*th IEEE Conf. on Decision and Control*, 2007, pp. 4924–4931.

[5] M. Uliana, F. Andreucci, and B. Papalia, "The navigation system of an autonomous underwater vehicle for antarctic exploration," in *OCEANS '97. MTS/IEEE Conference Proceedings*, vol. 1, oct 1997, pp. 403 – 408 vol.1.

[6] P. Bristeau, F. Callou, D. Vissière, and N. Petit, "The navigation and control technology inside the AR. drone micro UAV," in *IFAC World Congress*, vol. 18, no. 1, 2011, pp. 1477–1484.

[7] M. Pollefeys, L. Van Gool, M. Vergauwen, F. Verbiest, K. Cornelis, J. Tops, and R. Koch, "Visual modeling with a hand-held camera," *International Journal of Computer Vision*, vol. 59, no. 3, pp. 207–232, 2004.

[8] Z. Zhang and O. D. Faugeras, "Three-dimensional motion computation and object segmentation in a long sequence of stereo frames," *International Journal of Computer Vision*, vol. 7, pp. 211–241.

[9] S. Soatto, "3-d structure from visual motion: modeling, representation and observability," *Automatica*, vol. 33, pp. 1287–1312, 1997.

[10] S. Gupta, D. Aiken, G. Hu, and W. Dixon, "Lyapunov-based range and motion identification for a nonaffine perspective dynamic system," in *American Control Conference*, 2006, pp. 4471– 4476.

[11] R. Abdursul, H. Inaba, and B. K. Ghosh, "Nonlinear observers for perspective time-invariant linear systems," *Automatica*, vol. 40, no. 3, pp. 481–490, 2004.

[12] M. Sassano, D. Carnevale, and A. Astolfi, "Observer design for range and orientation identification," *Automatica*, vol. 46, no. 8, pp. 1369–1375, 2010.

[13] T. Hamel, R. Mahony, J. Trumpf, P. Morin, and M. Hua, "Homography estimation on the special linear group based on direct point correspondence," in *Conference on Decision and Control and European Control Conference (CDC-ECC)*, 2011, pp. 7902–7908.

[14] S. Soatto, P. Perona, R. Frezza, and G. Picci, "Motion estimation via dynamic vision," in *Decision and Control, 1994., Proceedings of the 33rd IEEE Conference on*, vol. 4, dec 1994, pp. 3253 –3258.

[15] R. Mahony and T. Hamel, "Image-based visual servo control of aerial robotic systems using linear image features," *Robotics, IEEE Transactions on*, vol. 21, no. 2, pp. 227–239, 2005.

[16] S. Izadi, D. Kim, O. Hilliges, D. Molyneaux, R. Newcombe, P. Kohli, J. Shotton, S. Hodges, D. Freeman, A. Davison *et al.*, "Kinectfusion: real-time 3d reconstruction and interaction using a moving depth camera," in *Proceedings of the 24th annual ACM symposium on User interface software and technology*. ACM, 2011, pp. 559–568.

[17] S. Bonnabel and P. Rouchon, "Fusion of inertial and visual : a geometrical observer-based approach," *2nd Mediterranean Conference on Intelligent Systems and Automation (CISA'09)*, vol. 1107, pp. 54–58, 2009.

[18] N. Zarrouati, E. Aldea, and P. Rouchon, "SO(3)-invariant asymptotic observers for dense depth field estimation based on visual data and known camera motion," in *American Control Conference, Montreal*, 2012, (arXiv:1103.2539v2).